Particle-water heat transfer during explosive volcanic eruptions

D. C. Woodcock,[1] J. S. Gilbert,[1] and S. J. Lane[1]

Received 17 February 2012; revised 29 August 2012; accepted 29 August 2012; published 11 October 2012.

[1] Thermal interaction between volcanic particles and water during explosive eruptions has been quantified using a numerical heat transfer model for spherical particles. The model couples intraparticle conduction with heat transfer from the particle surface by boiling water in order to explore heat loss with time for a range of particle diameters. The results are combined with estimates of particle settling times to provide insight into heat removal during eruption from samples of volcanic particles produced by explosive eruption. Heat removal is restricted by resistance to heat transfer from the volcanic particles with intraparticle thermal conduction important for large particles and surface cooling by boiling dominating for small particles. In most cases, volcanic particles approach thermal equilibrium with the surrounding fluid during an explosive eruption. Application of the results to a sample from the Gjálp 1996, Iceland eruption indicates that, relative to 0°C, 70–80% of the heat is transferred from the particles to boiling water during the settling time before burial in the stratigraphic succession. The implication is that, for subglacial explosive eruptions, much of the heat content of the magma is coupled into melting ice extremely rapidly. If all particles of the Gjálp 1996 deposit were cooled to the local boiling point by the end of the eruption then approximately 78% of the initial heat content was removed from the erupting magma during the eruption. This is consistent with calorimetric calculations based on volumes of ice melted during and after the eruption.

Citation: Woodcock, D. C., J. S. Gilbert, and S. J. Lane (2012), Particle-water heat transfer during explosive volcanic eruptions, *J. Geophys. Res.*, *117*, B10205, doi:10.1029/2012JB009240.

1. Introduction

[2] Hot volcanic particles may be cooled by heat transfer from particle surfaces by boiling water if they come into contact with liquid water or ice during an eruption. Volcanic activity in the presence of water may be explosive or non-explosive. Non-explosive activity includes the effusion of pillow lavas and sheet flows which largely maintain their integrity in contact with water; thus rates of magma-water heat transfer are mainly controlled by conduction through a solidified surface layer of increasing thickness [*Höskuldsson and Sparks*, 1997]. In contrast, explosive activity fragments magma to produce hot volcanic particles. The increased surface area allows greatly increased rates of magma-water heat transfer; these particles cool at rates that are increasingly controlled by surface heat transfer as size decreases. Particles may be produced by phreatomagmatic or magmatic fragmentation within wet environments. Such environments include both shallow subaqueous [*Kokelaar and Durant*, 1983] and deep subaqueous environments [*Head and Wilson*, 2003; *Allen and McPhie*, 2009], together with eruptions beneath ice sheets and glaciers [*Gudmundsson et al.*, 2004] and during magmatic intrusions into wet, unconsolidated sediments [*Skilling et al.*, 2002]. Hot particles produced by magmatic fragmentation in a dry environment may be transported during eruption to a wet environment: examples include spatter from Hawaiian-type eruptions landing onto ice, and pyroclastic density currents entering bodies of water [*Cas and Wright*, 1991] or flowing over ice surfaces [*Pierson et al.*, 1990].

[3] The particle-water heat transfer processes will be similar whenever hot volcanic particles contact water. It is difficult to infer heat transfer rates during subaqueous eruptions because the heat of the eruption is rapidly dispersed through a large volume of water. In contrast, during subglacial eruptions (Figure 1) the heat of eruption melts ice: heat transfer rates may be inferred by calorimetry from repeated observation of the ice surface above the eruption site and, in the case of the predominantly subglacial Gjálp 1996 (Iceland) eruption, by the flow of meltwater from the eruption site [*Gudmundsson*, 2003].

[4] In this paper we: (1) develop a numerical heat transfer model for spherical particles that couples intraparticle thermal conduction with heat transfer from the particle surface by boiling water; (2) use this model to evaluate heat loss with time for a range of particle diameters, in particular to quantify cooling rates for particles produced during magmatic and phreatomagmatic eruptions; (3) combine the results with estimates of time available for cooling in order to quantify the heat removed during eruptions; (4) apply the results to samples

[1]Lancaster Environment Centre, Lancaster University, Lancaster, UK.

Corresponding author: D. C. Woodcock, Lancaster Environment Centre, Lancaster University, Lancaster LA1 4YQ, UK. (d.woodcock@lancaster.ac.uk)

0148-0227/12/2012JB009240

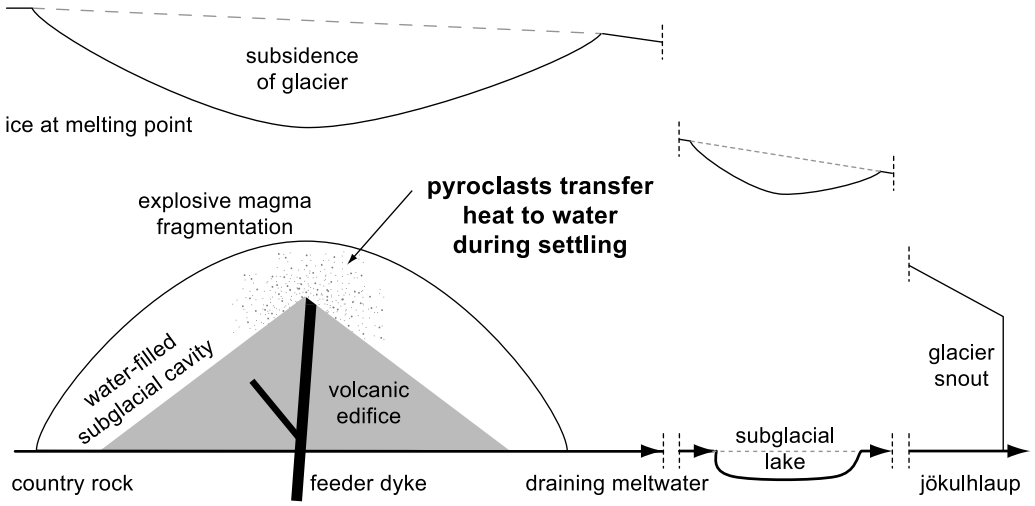

Figure 1. Schematic diagram (not to scale) of a subglacial explosive eruption together with potential drainage routes for meltwater. The transfer of heat from pyroclasts to water during settling forms the basis of this paper.

of known particle size distribution from both magmatic and phreatomagmatic eruptions, and (5) apply the results of this model to a sample with the same particle size distribution as material recovered from the 1996 Gjálp eruption [*Gudmundsson*, 2003] and compare the results of the heat transfer model with the determination of heat removal during the Gjálp eruption that was based on volumes of ice melted [*Gudmundsson et al.*, 2004].

1.1. Particle-Water Heat Transfer During Explosive Eruptions

[5] The rate of conductive heat loss from a spherical particle of diameter d and thermal diffusivity K to a constant temperature environment can be characterized by a thermal "diffusion time" t, where

$$t = \frac{d^2}{4K} \tag{1}$$

Gudmundsson [2003] applied this equation to a sample, with a mean particle diameter of 2 mm, recovered from the edifice that was produced during the Gjálp 1996 eruption. Assuming a thermal diffusivity of 10^{-6} m^2 s^{-1} [*Höskuldsson and Sparks*, 1997], the thermal diffusion time, during which a 2 mm diameter particle loses in excess of 90% of its heat [*Gudmundsson*, 2003], is around 1 s.

[6] The time required to cool a particle of a given size may be compared with the time available for cooling. *Gudmundsson* [2003] considered that the time available for cooling or the "exposure time" is the sum of a "settling time" while the particle is in transit and a "burial time" between landing and complete burial. *Gudmundsson* [2003] suggested settling times of 10–100 s and burial times of around 10 s in a water-filled subglacial cavity. The settling times are based on settling through a water depth of c. ten m at velocities of 0.1–1 m s^{-1}. These settling velocities are appropriate for particle sizes in the range 16–0.5 mm.

[7] The concept of thermal diffusion time (equation (1)) applies to the limiting case of instantaneous heat transfer from the surface of the particle to the surroundings. In practice, a hot particle immersed in water is likely to be covered by a film of steam for at least some of its cooling time which will restrict heat transfer. In this paper we demonstrate that some insight can be gained into heat transfer from pyroclasts to liquid water during settling by the use of a heat transfer model that combines intraparticle conduction with heat transfer from the particle surface by boiling water.

1.2. Heat Transfer by Intraparticle Conduction

[8] The equations for time-dependent heat loss by conduction from a spherical particle can be solved analytically for a variety of boundary conditions, including the cases of constant particle surface temperature [*Carslaw and Jaeger*, 1959] and constant surface heat transfer coefficient [*Lienhard and Lienhard*, 2008]. This approach was taken by *Birnie and Dyar* [1986] to calculate cooling rates for silicate glasses for various values of constant surface heat transfer coefficient.

[9] For other surface boundary conditions, including the case where surface heat flux varies with surface temperature, the problem must be solved by a numerical method. This is illustrated by *Thomas and Sparks* [1992], who studied heat loss from tephra particles by forced convection and radiation. *Keszthelyi and Denlinger* [1996] used a similar approach to study the cooling of pahoehoe flow lobes. *Mastin* [2007] calculated the rate of growth of glassy rinds during phreatomagmatic eruptions by assuming that surface heat loss was controlled by radiation and pool boiling, where the bulk velocity of the boiling liquid is zero relative to the hot surface. *Mastin* [2007] does not give details of the equations used for pool boiling heat transfer, nor does he appear to have considered flow (forced convective) boiling, where the boiling liquid has a bulk velocity relative to the hot surface.

[10] The study presented in this paper considers explicitly the variation of boiling heat transfer coefficient for the various boiling regimes encountered by a hot particle in contact with water for both pool and flow boiling. We incorporate these results into a model that helps to understand why, at the end of a subglacial eruption, a significant proportion of the eruption heat, relative to 0°C, is retained in the volcanic edifice. These results are based on the assumption that the

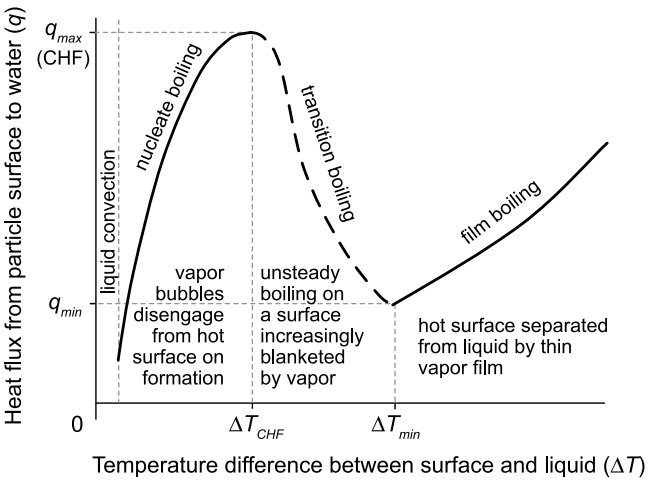

Figure 2. Variation of heat flux (q) from particle surface to water with temperature difference (ΔT) between hot surface and bulk liquid for different boiling regimes. The location of the critical heat flux (CHF) is indicated by $q_{\max}$ and ΔT_{CHF}.

bulk liquid (i.e., the subglacial cavity water) surrounding the particle surface is at its boiling point.

1.3. Heat Transfer by Boiling

[11] This section outlines the processes involved during heat transfer from a hot surface by boiling water. Figure 2 shows, in schematic form, the variation in boiling "heat flux" (q) with temperature difference (ΔT) between the surface and the liquid boiling point, together with the resulting boiling heat transfer "regimes."

[12] Nucleate boiling, when vapor disengages from the hot surface as bubbles, occurs for low values of ΔT above the minimum needed for bubble nucleation. Heat flux increases rapidly with ΔT until a maximum or "critical" heat flux (CHF) is reached. The nucleate boiling regime is well characterized because of its importance in the chemical and power generation industries. The location of the CHF is of utmost importance to the designers of steam generation equipment because operation at a heat flux greater than the CHF is only possible in the film boiling regime, where the high surface temperature would cause rapid equipment failure ("burnout") due to overheating of the heat transfer surface. Nucleate boiling research has been carried out for both pool boiling and for flow boiling conditions [*Whalley*, 1987].

[13] Beyond the CHF, heat flux decreases with ΔT to a minimum ($q_{\min}$ in Figure 2) in a "transition boiling" regime where unsteady boiling occurs on a surface that is increasingly blanketed by vapor. Designers of steam generation equipment tend to avoid this region, with its non-intuitive behavior, thus the heat transfer equations for transition boiling are poorly constrained.

[14] For a surface temperature above $\Delta T_{\min}$ (the temperature difference at $q_{\min}$ in Figure 2), a stable "film boiling" regime becomes established where heat flux increases with temperature and the hot surface is separated from the liquid by a thin vapor film. Heat transfer equations for film boiling in both pool and forced convective environments are well established [*Bromley*, 1950; *Bromley et al.*, 1953; *Lienhard and Lienhard*, 2008]. Although the heat transfer resistance is relatively high in this regime, the high ΔT can drive high heat fluxes, particularly at high surface temperatures.

[15] Figure 2 demonstrates that, during boiling heat transfer, the surface heat flux varies with ΔT and thus with the particle surface temperature. We incorporate this variation into a heat transfer model to quantify cooling rates for volcanic particles interacting with water.

2. Method

[16] The coupled intraparticle conduction-surface boiling heat transfer model calculates the cooling time required for a particle to lose a given percentage of its initial heat content relative to the local water temperature. We assume spherical, non-porous particles with temperature-independent thermal properties that are cooled by water at its boiling point. We consider the effect of these assumptions later in the paper.

2.1. Development of an Intraparticle Conduction Model

[17] Time-dependent heat loss by conduction is described by the heat conduction equation [*Carslaw and Jaeger*, 1959]:

$$\frac{\partial T}{\partial t} = K\nabla^2 T \tag{2}$$

where T is the temperature in the particle at time t and K is the particle thermal diffusivity.

[18] Our model for intraparticle conduction was developed by using the "control volume" method [*Kreith and Bohn*, 1993; *Incropera and DeWitt*, 1996]. This method carries out an unsteady state heat balance on an elemental spherical shell to generate an explicit difference equation that can be solved numerically. The choice of size for the radial step length is a compromise between accuracy and computation time. The time step was chosen to satisfy the Courant condition for stability [*Anderson*, 1995]. The physical properties of the particles used in the model are listed in Table 1.

[19] The model determines the radial temperature variation, and hence the proportion of heat lost, with time for a given particle diameter. Our model has been validated by comparison with analytical solutions presented in the literature for the case of a constant surface heat transfer coefficient, [*Incropera and DeWitt*, 1996; *Lienhard and Lienhard*, 2008]. Details of the model validation are presented in Appendix A.

2.2. Modeling of Heat Transfer From the Particle Surface by Boiling Water

[20] Boiling heat fluxes depend on the temperature difference between the particle surface and the bulk liquid (Figure 2). The heat flux versus temperature difference

Table 1. Physical Properties of Particles Used in Model

Property	Values		Units
	Basaltic	Rhyolitic	
Thermal diffusivity[a]	1×10^{-6}	3×10^{-6}	$m^2\ s^{-1}$
Density[a]	2700	2300	$kg\ m^{-3}$
Specific heat capacity[a]	1089	1049	$J\ kg^{-1}\ K^{-1}$
Emissivity	0.97[b]	0.97	Dimensionless

[a]From *Höskuldsson and Sparks* [1997].
[b]From *Ball and Pinkerton* [2006].

Table 2. Physical Properties of Water Used in Model[a]

Property	Value				Units
	at 0.1 MPa	at 0.5 MPa	at 2 MPa	at 6 MPa	
Boiling point	99.6	151.8	212.4	275.6	°C
Vapor density	0.59	2.67	10.0	28.1	kg m^{-3}
Liquid density	958	910	853	750	kg m^{-3}
Vapor specific heat capacity	2010	2300	3070	4750	J kg^{-1} K^{-1}
Liquid specific heat capacity	4220	4330	4560	5200	J kg^{-1} K^{-1}
Vapor thermal conductivity	2.5×10^{-2}	3.0×10^{-2}	3.9×10^{-2}	5.9×10^{-2}	W m^{-1} K^{-1}
Liquid thermal conductivity	6.8×10^{-1}	6.9×10^{-1}	6.6×10^{-1}	5.8×10^{-1}	W m^{-1} K^{-1}
Vapor viscosity	1.2×10^{-5}	1.4×10^{-5}	1.6×10^{-5}	1.8×10^{-5}	Pa s
Liquid viscosity	2.8×10^{-4}	1.8×10^{-4}	1.3×10^{-4}	9.7×10^{-5}	Pa s
Latent heat of vaporization	2260	2110	1890	1570	kJ kg^{-1}
Surface tension	5.9×10^{-2}	4.8×10^{-2}	3.5×10^{-2}	2.0×10^{-2}	N m^{-1}

[a]All data from *Rogers and Mayhew* [1980] except surface tension and liquid density (from *Incropera and DeWitt* [1996]).

equations used in our model have been distilled from the engineering literature and are presented in Appendix B. These equations assume that the bulk liquid surrounding the hot surface is at its local boiling point (a condition known as "saturation"). When the water is below its boiling point (i.e., subcooled), *Lienhard and Lienhard* [2008] indicate that boiling heat fluxes are increased compared with water at its boiling point for the same temperature difference between the hot surface and the bulk liquid; however the appropriate heat transfer equations for subcooled boiling have not been developed. The assumption of saturated boiling should give an upper bound on cooling times required. The thermal and transport properties for water used in the model are listed in Table 2.

[21] The equations in Appendix B would consume excessive computation time if embedded directly into the model. For a given particle diameter and water pressure, the heat transfer coefficients were evaluated for the nucleate boiling and film boiling regimes, using the appropriate liquid and vapor thermal and transport properties for water (Table 2). The corresponding heat flux versus temperature difference variation for each regime was then fitted to an equation that was used directly to replace the surface boundary condition in the intraparticle conduction model.

3. Results

3.1. General Results

[22] This section explores results from the coupled intraparticle conduction-surface boiling model. The first part of this section looks at the effect of the surface heat transfer resistance on the cooling of individual particles of different diameter. The sensitivity of the surface heat transfer resistance to boiling type and water pressure is explored in the second part. The third part examines the extent of heat removal from individual particles of different diameter in a given time. The final part considers samples of volcanic deposits by exploring the extent of heat removal in a given time for samples with known particle size distributions. All results are for basaltic particles cooling from 1150°C unless otherwise stated.

3.1.1. The Effect of Particle Surface Heat Transfer Resistance

[23] Table 3 shows the times required for particles to lose 98% of their initial heat content, relative to the local bulk water temperature, for the cases where (1) there is instantaneous surface heat transfer and (2) surface heat transfer is appropriate to flow boiling of water at a pressure of 2 MPa, equivalent to a water depth of around 200 m.

[24] Table 3 shows the Biot number for each particle, assuming a surface heat transfer coefficient of 1.5 kW m^{-2} K^{-1}, a value appropriate for film boiling. Small particles have low Biot numbers: the cooling rates for small particles are thus controlled by surface heat transfer. However, small particles cool very quickly and retain little heat in a typical volcanic sample. In contrast, large particles cool slowly and contribute a significant proportion of the heat remaining after burial. Similar results have been found for the forced convective cooling of pyroclasts in air [*Thomas and Sparks*, 1992; *Capaccioni and Cuccoli*, 2005].

[25] Figure 3 shows radial temperature profiles at selected values of percentage heat removal, together with the variation of surface temperature with time, for both small (2 mm) and large (32 mm) diameter particles. Cooling rates for small particles are controlled by surface heat transfer. It follows that intraparticle radial temperature profiles are flat (Figure 3a) and that, in the context of boiling at the particle surface, heat transfer is predominantly by film boiling (Figure 3b). In contrast, heat transfer from large particles is dominated by intraparticle conduction. Consequently surface temperatures are reduced (Figure 3a) and surface film boiling is replaced by nucleate boiling at a much earlier dimensionless time as the particle progressively cools (Figure 3b).

Table 3. Times for Spherical Particles of Various Diameters to Lose 98% of Their Initial Heat Content Relative to 212°C

	Particle Diameter (mm)		
	32	8	2
"98% cooling time"/s for:			
(1) no surface resistance[a]	85	5.3	0.33
(2) boiling water, 2 MPa[b]	98	8.8	1.1
Ratio of cooling times (2) to (1)	1.15	1.7	3.4
Biot number[c] for U = 1.5 kW m^{-2} K^{-1}	8.8	2.2	0.5

[a]Results from *Lienhard and Lienhard* [2008].
[b]Results from numerical model; flow boiling with fluid velocity equal to particle terminal velocity.
[c]Defined as $U\,d/2\,k$, where U, d and k are the particle surface heat transfer coefficient, diameter and thermal conductivity respectively [*Lienhard and Lienhard*, 2008].

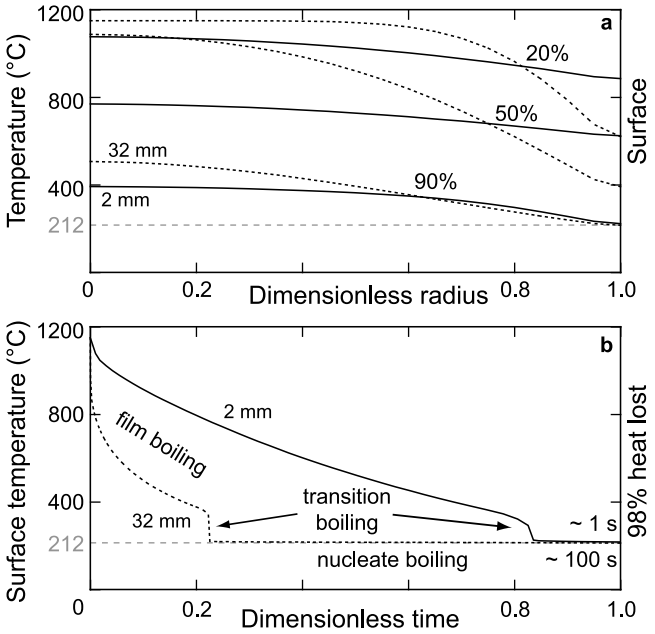

Figure 3. (a) Radial temperature profiles are shown at selected values (20, 50 and 90) of percentage heat transferred to the cavity water from 2 mm (solid lines) and 32 mm (dashed lines) diameter volcanic particles. Dimensionless radius (=r / r_o) is the ratio of radial position within the particle to the particle radius. (b) The surface temperature is shown as a function of dimensionless time for the same particle sizes. The regions of surface temperature where heat transfer is controlled by film, transition and nucleate boiling (Figure 2) are shown for both particle sizes. Dimensionless time is the ratio of elapsed cooling time to the time required to transfer 98% of a particle's heat to the surrounding water (∼1 s for 2 mm particles and ∼100 s for 32 mm particles). Results are from the numerical model, assuming basaltic particles initially at 1150°C cooled by flow boiling of water at 2 MPa (212°C).

3.1.2. Sensitivity of Surface Heat Transfer to Boiling Water Pressure and Boiling Type

[26] Figure 4 illustrates the effect of pressure on cooling times required during flow boiling. Cooling times decrease at higher pressures as expected from boiling heat transfer theory, with a greater sensitivity for small particle diameters. The prominent inflexion in the curve for 0.1 MPa in Figure 4b is produced by the change from a film boiling regime to a nucleate boiling regime at around 80% heat removal.

[27] Flow boiling calculations assumed that the bulk water velocity relative to the particle surface was equal to the particle terminal velocity during settling. This situation is probably appropriate while the particle is "settling" through the water. During the subsequent burial time, the particle surface is likely to experience decreasing water velocities as it becomes progressively buried. Figure 4 compares the cooling times required for flow boiling with times for pool boiling conditions at 2 MPa. Cooling times are shorter for flow boiling, reflecting the convective enhancement of the boiling heat transfer process.

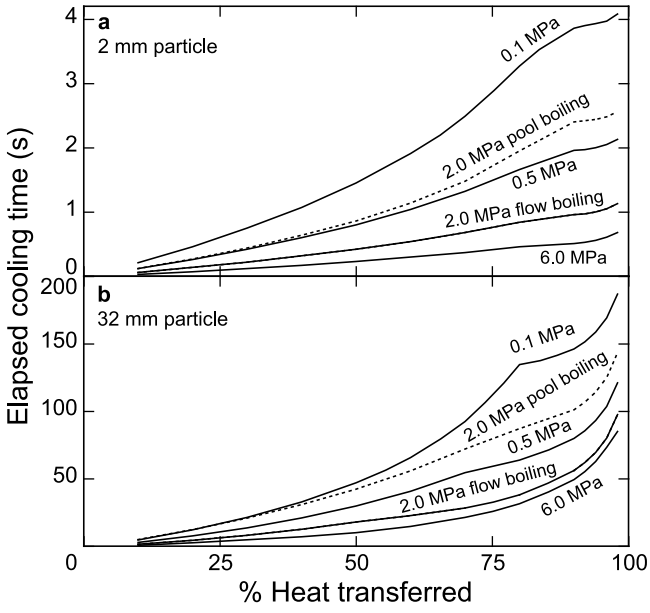

Figure 4. The percentage of heat transferred by flow-boiling (solid lines) from (a) 2 mm, and (b) 32 mm, particles to water at the specified pressure boiling point is plotted as a function of elapsed cooling time. Pool boiling conditions (dashed lines) are compared for a pressure of 2 MPa, illustrating the effectiveness of forced convection in increasing cooling rates.

3.1.3. The Extent of Heat Removal From Individual Particles in a Given Settling Time

[28] The numerical model calculates heat loss with time for a given particle diameter. Figure 5 summarizes the results of such calculations for basaltic particles as a family of curves

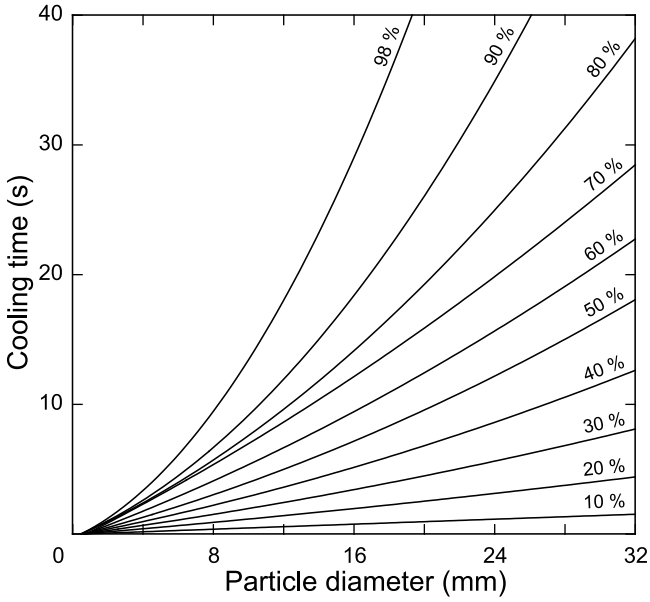

Figure 5. Particle cooling times, as a function of particle diameter, required for the indicated percentage removal of heat relative to a water temperature of 212°C, which is the boiling point at 2 MPa. Heat transfer is by flow boiling during particle settling.

Table 4. Percentage Heat Removal[a] for Various Particle Sizes, Relative to a Water Temperature of 212°C[b], for a Range of Settling Times

	Particle Diameter (mm)					
	32	16	8	4	2	<2
2 s settling time	12	20	42	83	99	>99
5 s settling time	21	38	78	>99	>99	>99
10 s settling time	35	61	98	>99	>99	>99
20 s settling time	55	86	>99	>99	>99	>99
50 s settling time	87	99	>99	>99	>99	>99
100 s settling time	98	100	>99	>99	>99	>99

[a]From basaltic particles with an initial temperature of 1150°C. All results are for flow boiling.
[b]The boiling point at 2 MPa.

that show the cooling time required, versus particle diameter, to remove various proportions of heat relative to the cavity water temperature. Figure 5 was developed for flow boiling conditions, which is appropriate while the particle is settling through water before burial. We define settling time as the period from the initial contact of a particle with water to the time when the particle begins to become buried. If a settling time versus particle diameter line could be added to Figure 5, it would be possible to read off, for each particle diameter, the percentage removal of heat before burial of the particle.

[29] Table 4 records the percentage heat removal, relative to water temperature, for various particle sizes and settling times. Table 5 shows the percentage heat removal, relative to water temperature, for various particle sizes, compositions and boiling conditions, for a settling time of 20 s. Tables 4 and 5 demonstrate that small particles (<4 mm) will lose essentially all of their heat in less than 5 s.

3.1.4. The Extent of Heat Removal From Samples of Volcanic Particles

[30] In this section the results recorded in Tables 4 and 5 are applied to particle size distributions of volcanic samples to calculate the extent of heat removal from the samples in a given settling time. This is done for two cases: (1) using a theoretical particle size distribution that is based on the mechanics of the fragmentation process and (2) using sample volcanic particle size distributions.

[31] Particle fragmentation by explosion or impact produces a power law particle size distribution [*Kaminski and Jaupart*, 1998] in which the number (N) of fragments with radii greater than r_o is given by $N = \beta\, r_o^{-D}$, where

Table 5. Percentage Heat Removal[a] for Various Particle Sizes, Compositions and Boiling Conditions, for a Settling Time of 20 s

	Particle Diameter (mm)				
	32	16	8	4	<4
Basalt, flow boiling at 6 MPa[b]	68	91	>99	>99	>99
Basalt, flow boiling at 2 MPa	55	86	>99	>99	>99
Basalt, flow boiling at 0.5 MPa	39	65	99	>99	>99
Basalt, flow boiling at 0.1 MPa	32	49	80	>99	>99
Basalt, pool boiling at 2 MPa	28	56	98	>99	>99
Rhyolite[c], flow boiling at 2 MPa	82	98	>99	>99	>99
Rhyolite, flow boiling at 0.1 MPa	34	58	99	>99	>99

[a]Relative to boiling water at stated pressure.
[b]Equivalent to a water depth of 600 m.
[c]Initial temperature of 850°C.

Table 6. Results of Calculation of Percentage Heat Removed From a "Power Law" Particle Size Distribution

	Particle Diameter (mm)						
	32	16	8	4	2	<2	Total
Weight % in sample	9.1	9.1	9.1	9.1	9.1	54.5	100
% heat removed[a]	55	86	>99	>99	>99	>99	
Contribution %	5.0	7.8	9.1	9.1	9.1	54.5	94.6

[a]Basaltic particles, flow boiling at 2 MPa, 20 s settling time (Table 5).

β is a constant and D has a value of approximately three. For illustrative purposes, we assume a value of three for D: on a weight % basis this generates a "flat" particle size distribution that is independent of β. Table 6 shows such a particle size distribution with a mean particle diameter of 1 mm, together with the calculation of the percentage heat removal for a settling time of 20 s, assuming that the particles are basaltic and immersed in boiling water at 2 MPa. For each particle diameter, the contribution to the percentage heat removed from the sample is the product of the weight % of the particular particle diameter and the appropriate fractional heat removed (from Table 5). The percentage heat removed from the sample is then the sum of these contributions; in this case 94.6%. The calculations in Table 6 can be repeated for flow boiling at 0.1 MPa, when boiling heat transfer coefficients are much smaller (Figure 4). The percentage heat removed from the sample in this case is 87.4%. If the settling time is reduced to 2 s at 2 MPa, the percentage heat removed is 77.8%.

[32] *Stevenson et al.* [2011] presented particle size distributions of volcanic samples that were produced during different stages of a subglacial rhyolitic eruption.

[33] For illustrative purposes we use three of the particle size distributions in *Stevenson et al.* [2011]. These are summarized in Table 7. Lithofacies A was produced by phreatomagmatic explosive activity and has a median particle diameter of approximately 0.25 mm. Lithofacies C and D were produced by magmatic explosive activity and have median particle diameters of approximately 1 mm and 2 mm respectively. All lithofacies were likely erupted into a wet environment where the particles were cooled by interaction with water. Modification during transport and deposition may have caused the particle size distributions of these deposit samples to be different from the corresponding particle size distributions at the eruption site. However, the lithofacies are described as massive (Lithofacies A and D) or diffusely stratified (Lithofacies C), suggesting that there had been little sorting during transport and deposition. *Stevenson et al.* [2011] suggested that these lithofacies were probably deposited by density currents that flowed only a short distance (<500 m) from the eruption site.

Table 7. Particle Size Distributions[a]

	Particle Diameter (mm)						
	32	16	8	4	2	<2	Total
Lithofacies A weight %		1.6	1.5	3.0	3.4	90.5	100
Lithofacies C weight %		3.4	11.9	12.8	8.3	63.6	100
Lithofacies D weight %	6 .2	7.6	10.5	10.4	11.9	53.4	100

[a]From *Stevenson et al.* [2011].

Table 8. Percentage Heat Removed, Relative to Boiling Water, From Each Lithofacies Sample[a] for Various Settling Times and Pressures

		Percentage Heat Removal		
Settling Time (s)	Pressure (MPa)	A	C	D
20	2.0	>99.9	99.9	97.8
20	0.1	99.3	98.4	92.5
2	2.0	97.5	89.4	82.0
2	0.1	95.1	79.3	71.3

[a]From *Stevenson et al.* [2011].

[34] Table 8 shows the percentage heat removed from each lithofacies sample, for a number of combinations of settling times and pressures. The results in Table 8 indicate that a large part of the heat is removed even for settling times as short as 2 s.

[35] The boiling heat transfer equations used in the model assume that the bulk liquid surrounding the hot surface is at its local boiling point. We conclude that, if the water is at its boiling point, much of the heat from a sample of explosively produced volcanic particles is removed during a settling time of 20 s and that the average sample temperature approaches the temperature of the water into which the sample is erupted.

[36] When the water is below its boiling point, particles should continue to cool by single phase forced convection, once surface boiling ceases, for the remainder of the settling time. We have tentatively explored cooling under subcooled conditions by a modification to the model in which single phase forced convection cooling replaces saturated nucleate boiling when the nucleate boiling heat flux becomes lower than the single phase forced convection heat flux. Figure 6 shows a graph of cooling time versus percentage heat removal for a 16 mm diameter particle cooling in water at 2 MPa but subcooled to 0°C.

[37] Figure 6 shows that, for a 20 s settling time, heat removal is 84%, relative to 0°C water. This compares with 86% heat removal, relative to 212°C, for a particle of the same diameter cooling in water at its boiling point. We tentatively conclude that, for a given settling time, particles have a similar percentage heat removal, relative to the water temperature, whether the water is at its boiling point or is subcooled. We emphasize that the results in Figure 6 are approximate, because boiling on the particle surface has been modeled using the equations for saturated boiling. A more accurate model could be developed if suitable equations for subcooled boiling heat transfer from spheres can be obtained. Even so, the implication of Figure 6 is that the model would give no insight into the temperature of the cavity water into which the particles were erupted.

3.1.5. Applicability of the Model

[38] Our coupled intraparticle conduction - surface boiling model is applicable to any situation in which a hot spherical particle is immersed in water. It should also be applicable to a situation where a hot particle is in contact with liquid water or ice provided that the particle surface remains wet during cooling. The model has been developed in some detail for the case of immersion in water at its boiling point and has been tentatively extended to the case of immersion in subcooled water. When applied to samples of explosively derived volcanic particles, the conclusion appears to be the same in both cases, in that much of the heat from a sample is removed during settling and that the average sample temperature approaches the temperature of the water into which the particles are erupted.

[39] Figure 7 indicates the range of applicability of the model on a phase diagram for pure water. Saturated boiling is represented by the line that connects the triple point (TP) with the critical point (CP). Within the supercritical region, surface heat loss will be by single phase convection of supercritical water; this mechanism may be relevant to subglacial explosive eruptions beneath very thick (>2300 m) ice or submarine eruptions at water depths exceeding approximately 3200 m [*Head and Wilson*, 2003]. We anticipate that the model could be extended to cover the supercritical region if required. The area labeled "liquid" on Figure 7 encompasses subcooled boiling, together with single phase liquid convection. This region is relevant to subaqueous explosive eruptions in general, although the locations of the phase boundaries would need to be modified for eruptions into saline solutions. In the remainder of the paper, we apply the model to explore the implications of particle-water heat transfer during the Gjálp 1996 subglacial eruption.

3.2. Application to the Gjálp 1996 Eruption

[40] The Gjálp eruption under the Vatnajökull ice cap, Iceland in October 1996 is one of the best-documented examples of a subglacial explosive eruption [*Gudmundsson et al.*, 1997; *Gudmundsson et al.*, 2004]; it thus provides data that can be used to constrain heat transfer models of subglacial eruptions. Continuous tremor at the site of the eruption began at around 2200 h UTC on 30th September, marking the start of the eruption, and continued until the evening of 13th October. Penetration of the upper surface of the ice cap occurred around thirty hours after the start of the eruption and the resulting subaerial eruption produced a volcanic plume [*Gudmundsson et al.*, 2004]. The thermal output of this subaerial activity was estimated by

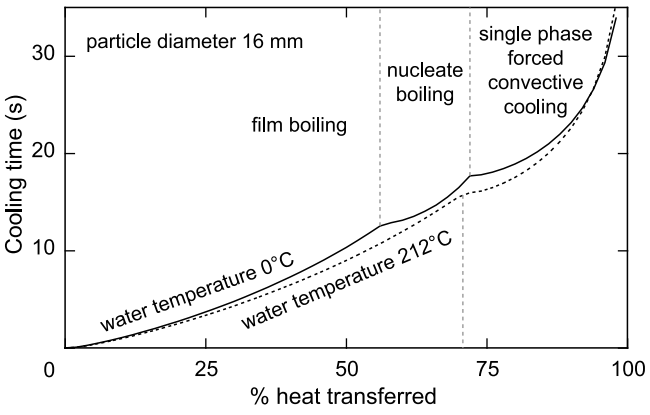

Figure 6. The solid line shows cooling time required versus percentage heat transferred (relative to water temperature) for a 16 mm diameter particle cooling in water at 2 MPa and subcooled to 0°C. The dashed line shows the corresponding behavior for cooling in water at 212°C, the boiling point at 2 MPa. This model tentatively suggests that, relative to water temperature, the proportion of heat transferred from a pyroclast during settling in water is almost independent of water temperature.

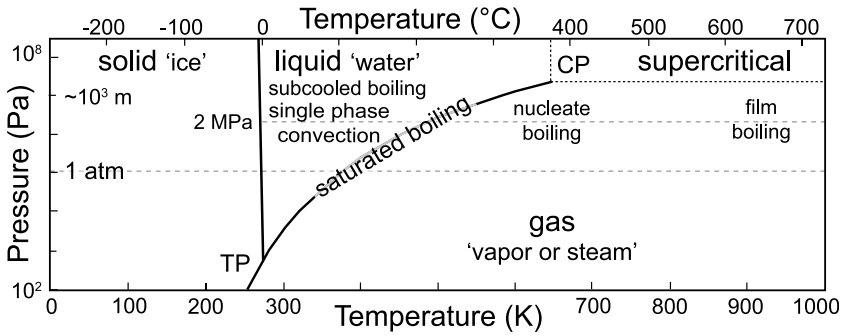

Figure 7. Phase diagram for pure water indicating the range of applicability of the model. Saturated boiling, when the bulk water is at its boiling point, is represented by the line that connects the triple point (TP) with the critical point (CP). Subcooled boiling occurs within the liquid field. A pyroclast in liquid water whose surface temperature falls in the vapor field will cool by two-phase boiling heat transfer. The example at 2 MPa initially cools by film boiling, changing to nucleate boiling as surface temperature reduces. With a surface temperature in the liquid or supercritical field, cooling is by single phase convection.

Gudmundsson et al. [2004], using an empirical relationship between plume height and thermal output [*Sparks et al.*, 1997]. Overall, subaerial activity during the eruption accounted for 2–4% of the thermal output; thus almost all of the heat in the magma was transferred subglacially to melt the ice both during and after the eruption [*Gudmundsson et al.*, 2004]. Melting of ice by the eruption produced depressions in the glacier surface above the eruption site. The development of these depressions was monitored by repeated airborne radar altimetry observation.

[41] Meltwater produced during the eruption drained into the subglacial lake Grimsvötn, to the south of Gjálp, where it accumulated until release in early November 1996. An independent second method of monitoring ice melting rates comprised the determination of changes in the volume of water in Grimsvötn from changes in the lake level (measured by repeated airborne radar altimetry of the surface of the floating ice) and the known lake bathymetry [*Gudmundsson et al.*, 1997]. Comparison of the results of both methods [*Gudmundsson et al.*, 2004, Figure 9a] shows no systematic lag between surface deformation and Grimsvötn water level on the timescale of the observations.

[42] Table 9 shows the total volume of ice melted at various times during and subsequent to the eruption [*Gudmundsson et al.*, 2004]. The entries up to and including 11th November 1996 are based on changes in the volumes of depressions in the glacier surface formed during and immediately after the eruption, together with the volume of the volcanic edifice. The volume of the edifice was determined by a combination of radar echo sounding and gravity survey together with visual observation of sections of the ridge crest while it was exposed [*Gudmundsson et al.*, 2002]. The depressions in the glacier surface include those above the eruption location, above the subglacial passage of meltwater into Grimsvötn, adjacent to Grimsvötn, and above the subglacial passage of the jökulhlaup out of Grimsvötn on 5th–6th November, when water emerged at freezing point from the glacier margin, some 50 km from Grimsvötn [*Tweed et al.*, 2005]. Entries in Table 9 for the longer post-eruption period are based on changes in the glacier surface above the eruption site, corrected for ice addition by precipitation.

[43] A total of 2.91 km^3 of ice had been melted by 12th October, a day before the end of the eruption. The heat above 0°C in the meltwater entering Grimsvötn during the eruption produced 0.3 km^3 of ice melting in a subglacial conduit (V_{p2} in *Gudmundsson et al.* [2004, Table 3]) when this water was released in the jökulhlaup from Grimsvötn on 5th–6th November. Thus, relative to 0°C, the heat removed during the eruption was equivalent to the melting of 3.21 km^3 of ice. Table 9 indicates that most of the residual heat in the eruption products had been removed by June 1998. An approximate proportion of the heat removed from the magma, relative to 0°C, averaged over the duration of the eruption, is thus 3.21/4.16 or 77%.

[44] The record of post-eruption cooling of the suglacial volcanic edifice was extended beyond June 1998 through to 2005 by *Jarosch et al.* [2008]. These authors carried out a detailed analysis of volume changes in the ice surface over the cooling edifice and made allowance for (1) the effects of relaxation of the depressions by ice inflow and (2) addition of ice from post-eruption precipitation. This study is considered by the authors to be more complete and thus provides a more reliable estimate of heat removed during the eruption than that reported in *Gudmundsson et al.* [2004]. *Jarosch et al.* [2008] conclude that approximately two thirds (67%) of the heat content of the magma (relative to 0°C) was removed during the eruption, with a further 20% by June 1997 and an additional 10% by June 2001, and that heat loss was insignificant from June 2001 up to June 2005.

[45] Fragmentation of magma by phreatomagmatic explosive activity during the Gjálp eruption should have produced small particles [*Zimanowski and Büttner*, 2003]. The

Table 9. Total Volume (V_t) of Ice Melted at Various Times Since the Start of the October 1996 Gjálp Eruption[a]

Date	30 Sep 1996	1 Oct 1996	3 Oct 1996	12 Oct 1996	11 Nov 1996	June 1997	June 1998
V_t (km^3)	0[b]	0.39[b]	1.50[b]	2.91[b]	3.75[c]	4.12[c]	4.16[c]

[a]From *Gudmundsson et al.* [2004].
[b]Period of eruption.
[c]Post-eruption period.

Table 10. Particle Size Distribution[a] of the Gjálp 1996 Eruption and Calculation of Heat Removed During Settling[b]

	Particle Diameter (d /mm)							
	>32	32	16	8	4	2	<2	Total
Weight % in sample	1.7	6.8	8.1	9.1	12.4	12.0	49.9	100
% heat removed	27	55	86	>99	>99	>99	>99	
Contribution %	0.5	3.7	7.0	9.1	12.4	12.0	49.9	94.6

[a]From *Gudmundsson* [2003].
[b]Relative to the local fluid temperature of 212°C; the boiling point of water at 2 MPa.

subsequent heat loss from the volcanic particles produced should have been rapid; however only 67% of the heat was removed, relative to 0°C, during the eruption. If all the magma was fragmented during eruption there are two likely reasons why heat removal relative to 0°C was incomplete on the timescale of the eruption. First, heat transfer could have been restricted by intraparticle conduction or by the heat transfer resistance of steam films on particle surfaces. Second, even if heat transfer between particle and the surrounding water were instantaneous, there would still have been a limitation due to the elevation of the ice cavity water temperature above 0°C [*Gudmundsson*, 2003]. We explore these reasons by applying our coupled intraparticle conduction – surface boiling model to the Gjálp 1996 eruption. This is done in two stages: by studying a "base case" in some detail and then by examining sensitivity to changes in the base case assumptions by means of a series of "step out" case calculations. A further reason why a third of the initial heat content of the magma remained in the edifice at the end of the eruption is that not all of the magma fragmented during eruption. A scenario with subcooled cavity water is consistent with the Gjálp eruption data if the eruption edifice contains significant amounts of effusive and intrusive material that cooled slowly; we discuss this in Section 4.

3.2.1. "Base Case" Calculations: Surface Heat Transfer by Boiling at 2 MPa

[46] The base case calculations make the following assumptions: (1) the volcanic particles have an initial temperature of 1090°C, based on a temperature of 1090 +/− 50°C for the Gjálp 1996 eruption products [*Gudmundsson et al.*, 1997], (2) the particle settling time is 20 s, which is at the lower end of the range of settling times suggested by *Gudmundsson* [2003], (3) the cavity pressure is 2 MPa and (4) the percentage heat removal versus particle diameter data for the basaltic andesite (Icelandite) of the Gjálp eruption [*Steinthorsson et al.*, 2000] may be approximated by the data for basaltic particles in Table 4.

[47] The average temperature of the cavity water is likely to have been in excess of the ice melting point. The temperature of meltwater leaving the eruption site was approximately 20°C averaged over the whole eruption but could have been considerably higher in the early stages [*Gudmundsson et al.*, 2004]. *Höskuldsson and Sparks* [1997] suggested temperatures of 50–100°C in convecting meltwater lenses for the case of heat loss from cooling pillow lavas. Considerably higher meltwater temperatures might be expected for explosive subglacial eruptions, where the heat flux from magma to water is much higher, and it is possible that meltwater temperatures may have approached or attained the boiling point appropriate to the cavity pressure, at least in the region local to the vent. For illustrative purposes we assume for the base case that particles are in contact with water at 212°C, the boiling point at 2 MPa.

[48] Data from Table 4 can be used to estimate the heat removed before burial from a hyalotuff that has the same particle size distribution as the samples recovered from the edifice that was produced during the Gjálp 1996 eruption. Sampling took place in June 1997, when the top of the edifice was exposed at the surface [*Gudmundsson*, 2003]. We assume that this sample is representative of the volcanic particles that were produced during the subglacial eruption. Table 10 shows the particle size distribution in weight % for size ranges centered on the stated particle diameter, the appropriate percentage heat removal data from Table 4 and the resulting contribution of each size range to the total percentage heat removed from the sample.

[49] The heat transfer model result in Table 10 indicates that 94.6% of the heat in the Gjálp sample, relative to a local cavity water temperature of 212°C, was removed from particles before burial during the eruption. The heat transfer model assumed a constant specific heat capacity for the Gjálp sample over the entire potential cooling range from 1090°C to 212°C. The mean temperature, T_e of 259°C for the sample before burial can be obtained from the equation $(1090 - T_e) / (1090 - 212) = 0.946$. If the Gjálp sample is representative of the whole volcanic edifice then, relative to 0°C, the heat transfer model indicates that the percentage heat removal during the settling time is thus $100 \times (1090 - 259) / 1090$ or 76%. A repeat of these heat transfer model calculations with the settling times halved and doubled gave heat removal values of 73% and 79% respectively, showing that percentage heat removal is relatively insensitive to settling time.

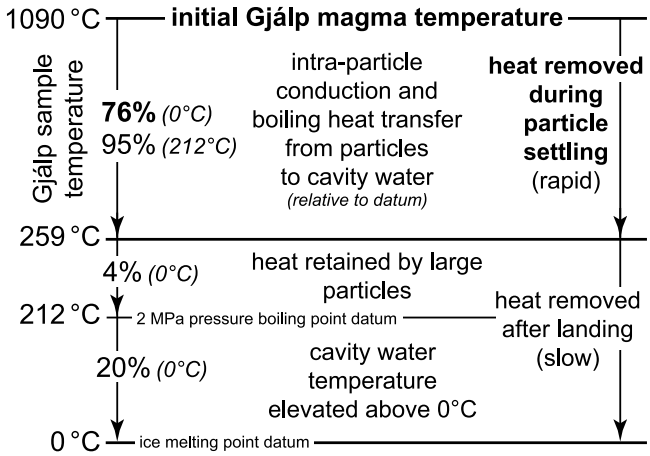

Figure 8. Comparison of heat removed during particle settling with heat removed after landing for the Gjálp sample (Table 10). Relative to 0°C, the sample lost 76% of its initial heat content during settling as it cooled from 1090°C to 259°C and 95% relative to 212°C. Heat removal was restricted by resistance to heat transfer from particles to water (at 212°C) and limited by the elevation of the local temperature of the meltwater in the ice cavity above 0°C. The residual heat in the sample was removed much more slowly during the burial and post-burial period until the end of the eruption and subsequently during the post-eruption period [*Jarosch et al.*, 2008].

Table 11. Comparison of Percentage Heat Removed for "Step Out" Case Conditions (Marked Δ) With Base Case Conditions

Case	Cavity Pressure	T_b	Percentage Heat Removal[a]	
			Relative to 0°C	Relative to T_b
Base case	2 MPa	212°C	76	95
Δ Cavity pressure	6 MPa	276°C	73	91
Δ Cavity pressure	0.1 MPa	100°C	72	89

[a]For 20 s settling time.

Figure 8 shows that heat removal before burial relative to 0°C is both restricted by resistance to heat transfer from particles to cavity water and limited by elevation of the temperature of the meltwater in the ice cavity above 0°C, although elevation of meltwater temperature appears to dominate.

3.2.2. Sensitivity Analysis

[50] This section explores the sensitivity of percentage heat removal to changes in the base case assumptions by means of "step out" case calculations. The results of these calculations, together with the original base case results, are presented in Table 11 and discussed below. Changes to cavity water temperature and pressure are emphasized as these appeared to be the dominant control in the base case.

[51] The cavity water pressure assumed in the base case is equivalent to a glaciostatic pressure of around 200 m of ice; conditions that would be attained part way through the Gjálp subglacial eruption. The heat transfer calculations were repeated for a pressure of 6 MPa (and a corresponding boiling point of 276°C), appropriate to an ice thickness of around 600 m at the start of the Gjálp eruption [*Gudmundsson et al.*, 2004]. Comparison of the results (Table 11) with the base case show a small reduction in percentage heat removed (relative to 0°C), although this is wholly due to the increased cavity water temperature. The calculations were repeated for a pressure of 0.1 MPa, appropriate to subaerial activity toward the end of the eruption [*Gudmundsson et al.*, 2004]. Comparison of these results with the base case show a small reduction in percentage heat removed (relative to 0°C), although in this case this is due to the large reduction in boiling heat transfer coefficients at the lower pressure (Figure 4).

3.2.3. Variation of Particle Properties With Temperature

[52] The base case and "step out" cases evaluated in Section 3.2.1 and 3.2.2 assumed constant (temperature-independent) particle properties. This section explores the effect of the variation of particle density, thermal conductivity and specific heat capacity with temperature.

[53] *Murase and McBirney* [1973] report data on the temperature variation of density and thermal conductivity of a tholeiitic basalt. Density decreased by 6% from 20°C to 1200°C, while thermal conductivity decreased by around 50% over the same temperature range. The temperature variation of density and thermal conductivity is assumed to be similar on a percentage basis for the basaltic andesite (Icelandite) [*Steinthorsson et al.*, 2000] composition of the Gjálp sample.

[54] The variation of specific heat capacity with temperature was determined for a glass with the composition of the Gjálp sample [*Steinthorsson et al.*, 2000] using the method outlined in *Spera* [2000]. Specific heat capacity is predicted to increase from 650 J kg^{-1} K^{-1} at 0°C to 1316 J kg^{-1} K^{-1} at 1090°C. This variation implies that, compared with the use of an average value of 1089 J kg^{-1} K^{-1} in the base case, a greater proportion of heat is removed at a higher temperature. Particles should thus attain a given percentage heat removal more quickly when modeled with a temperature-dependent specific heat capacity.

[55] A quadratic fit of specific heat capacity versus temperature, together with a linear fit of density and thermal conductivity with temperature, was incorporated into a modified version of the numerical heat transfer model. This modified model was run with all other conditions identical to the base case. The resulting percentage heat removed (relative to 0°C) of 81% is slightly larger than that of the base case value of 76%.

4. Discussion

[56] In the previous sections a new numerical heat transfer model for spherical particles that combined intraparticle conduction with heat transfer from the particle surface by boiling water was developed. This model was used to explore heat loss with time for a range of particle diameters for eruption into water at its boiling point. The results were combined with estimates of settling times in order to quantify the heat removed during eruption and the results applied to samples of known particle size distribution from both magmatic and phreatomagmatic eruptions.

[57] The results were applied to a sample of the Gjálp 1996 deposit and a number of "step out" cases were explored in order to test the sensitivity of the results to the assumptions made. The results of these calculations are summarized in Table 11 and indicate a percentage heat removal during particle settling time, relative to 0°C, of 70–80%. This can be compared with the 67% determined from the calculations based on ice volumes melted during the eruption. Figure 8 shows that heat removal during settling time is restricted by resistance to heat transfer from particles to water and limited by the elevation of the local temperature of the meltwater in the ice cavity above 0°C. Elevation of water temperature in the ice cavity is the dominant control. These results assume that all of the magma fragmented to produce a population of volcanic particles which approached thermal equilibrium with the surrounding water. Rapid cooling of small volcanic particles to the local boiling point is thus one possible scenario that is consistent with the Gjálp eruption data.

[58] A scenario with subcooled cavity water is consistent with the Gjálp eruption data if the eruption edifice contains significant amounts of effusive and intrusive material that cooled slowly. The initial stage of the eruption may have been effusive, with the emplacement of basal layers of pillow lavas [*Gudmundsson*, 2003]. In addition, intrusions, as dykes or as layers or lobes of pillow lavas within a subglacial edifice, are a common but minor component of magmatic activity during the growth of an edifice [*Jakobsson and Gudmundsson*, 2008]. *Gudmundsson et al.* [2002] suggested that up to a third of the volume of the Gjálp edifice may consist of pillow lavas. Heat loss from intrusions and basal pillow lava layers is likely to be much slower, with significant heat retained beyond the end of the eruption. *Gudmundsson* [2003] indicated that the proportion of the initial heat content removed

from a layer of pillow lavas before burial ranges from 10% to 45%, depending on the effusion rate. A combination of a proportion of non-fragmented material and an elevated cavity fluid temperature, but significantly below boiling point, is probably the most likely scenario for the Gjálp eruption. The remainder of this section reviews some of the assumptions of our model.

4.1. The Effect of Particle Morphology

[59] The heat transfer model assumes spherical particles; volcanically produced particles have more complex morphologies and the assumption of spherical particles needs further consideration. For a given volume, a sphere has the smallest surface area and the longest "thermal conduction path" from center to surface. The assumption of spherical particles in the model should thus give an upper bound on cooling times.

[60] Our model assumes that particles are non-porous. The vesicularity of volcanic particles is determined by the extent of magmatic degassing before magma-water interaction [*Cioni et al.*, 1992]. A vesicular particle has a smaller thermal capacity than a non-vesicular particle of the same size; however the heat conduction path has both a smaller area and a greater tortuosity. Measurements by *Bagdassarov and Dingwell* [1994] on vesicular rhyolites with 70–80% porosity indicated thermal diffusivities around three times lower than for the equivalent non-vesicular material. The effect on cooling times should thus be broadly similar to that due to the difference in thermal diffusivity between basaltic and rhyolitic particles (Table 1).

4.2. Cooling Time Revisited: Post-Burial Heat Transfer

[61] So far we have quantified heat loss from a particle during its settling time. Our calculations have shown that, for all but the largest particles, heat loss is rapid during the settling time, even though the duration is short, typically 10 to 100 s. In contrast, in the case of the Gjálp 1996 eruption, the post-burial period until the end of the eruption was typically days long when low rates of heat transfer may have produced additional particle cooling within the deposit.

[62] During the post-burial period, heat transfer will be coupled to the flow of pore fluid through the permeable strata of the cooling volcanic edifice. We recognize that calculation of heat transfer under these conditions is not trivial but we attempt to obtain some indication of the extent of post-burial particle cooling by considering a limiting case of a particle in a stagnant fluid. In this scenario, the Nusselt number, Nu, is equal to two [*Incropera and DeWitt*, 1996], where $Nu = U\,d/k_f$, U is the particle surface heat transfer coefficient, d is the particle diameter and k_f is the thermal conductivity of the fluid phase surrounding the particle. The corresponding Biot number is given by the ratio k_f/k, where k is the particle thermal conductivity. When the pore space is filled with liquid water the Biot number is 0.2; the corresponding value for steam-filled pores is 0.02. In both cases the Biot number confirms that heat transfer is limited by the surface thermal resistance. Application of unsteady state theory [*Incropera and DeWitt*, 1996] indicates that under these conditions a 30 mm diameter particle will lose 90% of its excess heat in around 0.5 h in liquid water and 4 h in steam. The corresponding times for a 100 mm particle are around 5 and 40 h respectively. Thus it seems likely that the temperature of all particles will approach thermal equilibrium with the local fluid by the end of an eruption.

[63] If all particles are cooled to the local fluid temperature, then the proportion of heat removed during the eruption, relative to 0°C, is determined solely by the elevation of the local fluid temperature above 0°C. The proportion of heat removed during the eruption may be estimated if the fluid is at its local boiling point throughout the volcanic edifice at the end of the eruption. This can be done by considering successive elements of the edifice and estimating the appropriate saturation temperature, assuming hydrostatic or glaciostatic conditions as appropriate. This procedure has been applied to the Gjálp 1996 eruption, using data in *Gudmundsson et al.* [2002]. The volume-averaged temperature of the edifice at the end of the eruption is approximately 235°C. Assuming a constant specific heat capacity of basaltic glass, the corresponding proportion of heat removed from the volcanic particles during the eruption, relative to 0°C, is thus (1090–235)/1090 or 78%. We note that our volume-averaged temperature of the edifice at the end of the eruption accords with the estimate made by *Jarosch et al.* [2008] on the basis of volumes of ice melted once allowance is made for the thermal capacity of the pore fluid in the edifice.

5. Conclusions

[64] A numerical heat transfer model has been developed for spherical particles that combines intraparticle conduction with heat transfer from the particle surface by boiling water. The model has been used to explore heat loss with time for a range of particle diameters for eruption into water at its boiling point and the results combined with estimates of settling time in order to quantify the heat removed during particle deposition. The principal conclusions are:

[65] 1. Heat transfer from small particles is dominated by surface film boiling. These particles are able to lose most of their initial heat content during the settling time before burial, even for settling times in the range 2–10 s. In contrast, heat transfer from large particles is dominated by intraparticle thermal conduction; they cool more slowly and thus contribute most to the heat retained on burial.

[66] 2. For a given settling time, particles appear to have similar percentage heat removal, relative to the water temperature, whether the water is at its boiling point or is subcooled.

[67] 3. Both resistance to heat transfer and elevated local water temperature control heat removal in the cooling time available before particle burial. Elevated water temperature appears to be the dominant control on pre-burial heat removal during eruption. Post-burial heat transfer may be significant for the remaining duration of the eruption; in this case elevated water temperature is the sole control on heat removal during eruption.

[68] 4. Application of the results to a sample of the Gjálp 1996 eruption product indicates that, relative to the local boiling point, 90–95% of the initial heat content was removed from the sample during the settling time before burial. Relative to 0°C, 70–80% of the initial heat content was removed from the sample during the settling time. This suggests that much of the heat content of the magma in the Gjálp 1996 eruption was rapidly coupled into melting ice,

Table A1. Comparison of Fractional Heat Removal: Our Model Versus Grober Chart[a]

Q / Q_i	$Bi^2\ Fo$	Fo	Cooling time (s)	Q / Q_i From Model	Model/ Grober Chart[b]
0.1	0.08	0.02	0.32	0.13	1.30
0.3	0.31	0.078	1.2	0.38	1.26
0.5	0.62	0.155	2.5	0.59	1.18
0.7	1.1	0.28	4.4	0.79	1.13
0.8	1.5	0.38	6.0	0.88	1.10
0.9	2.0	0.5	8.0	0.94	1.04
0.95	2.8	0.7	11.2	0.98	1.03

[a]From *Grober* [1961].
[b]Ratio of Q / Q_i from model (column 5) to Q / Q_i from Grober chart (column 1).

and this is likely to be the case for all subglacial explosive eruptions.

[69] 5. If all particles of the Gjálp 1996 deposit were cooled to the local boiling point by the end of the eruption then around 78% of the initial heat content was removed from the erupting magma during the eruption. This is consistent with calculations based on volumes of ice melted.

[70] 6. Rapid cooling of small volcanic particles to the local boiling point is one possible scenario that is consistent with the Gjálp eruption data. A scenario with subcooled cavity water is consistent with the Gjálp eruption data if the eruption edifice contains significant amounts of effusive and intrusive material that cooled slowly. This is probably the most likely scenario.

Appendix A: Validation of the Intraparticle Conduction Model

[71] This appendix documents a comparison of the results of our intraparticle conduction model with analytical solutions presented in the literature for the case of constant surface heat transfer coefficient.

[72] The analytical solution of the one-dimensional transient heat conduction equation with a constant surface heat transfer coefficient comprises a series solution with an infinite number of terms. An approximation to the exact solution, the Heisler-Grober chart [*Incropera and DeWitt*, 1996; *Lienhard and Lienhard*, 2008], is widely used for the solution of industrial transient heat transfer problems. The original Heisler chart [*Heisler*, 1947] presented the variation of temperature with time and position (radius in the case of a sphere). An additional chart was developed by *Grober* [1961] that presented the fractional heat loss from a body with time; this chart is used for validation of our model.

[73] The Grober chart is a dimensionless plot of fractional heat loss (Q/Q_i) against $Bi^2\ Fo$ with Bi as a parameter, where the Biot number $Bi = U\ r_o/k$, the Fourier number $Fo = K\ t/r_o^2$, U is the heat transfer coefficient at the particle surface, r_o, k and K are the particle radius, thermal conductivity and thermal diffusivity respectively and t is the cooling time required. The Fourier number can be considered as a dimensionless time variable. The chart is increasingly accurate as Fo increases, and deemed acceptable to engineering accuracy if $Fo > 0.2$ [*Incropera and DeWitt*, 1996].

[74] For the purpose of model validation, we ran the model with a particle radius of 4 mm, a particle thermal diffusivity of 10^{-6} m^2 s^{-1} and a particle thermal conductivity of 2.72 W m^{-1} K^{-1}. For a surface heat transfer coefficient of 1362 W m^{-2} K^{-1} the value of the Biot number was 2.0, corresponding to one of the family of curves presented on the Grober chart in *Incropera and DeWitt* [1996]. The values of $Bi^2\ Fo$ for a number of values of fractional heat loss (Q/Q_i) were obtained from the chart, and the resulting cooling times calculated. For each of these times the fractional heat loss was obtained from our model run. The results of this procedure are recorded in Table A1, together with the comparison between the fractional heat loss from our model and from the Grober chart. We note that the comparison (right hand column of the table) has values around unity and a tendency to unity with increasing Fo. This gives confidence that our intraparticle conduction model is valid.

Appendix B: Boiling Heat Transfer Equations

[75] This appendix documents the development of the heat flux versus ΔT equations used within the numerical model. Much of this appendix draws on the monograph of *Whalley* [1987].

B1. Nucleate Boiling Regime

[76] Nucleate pool boiling heat fluxes have been found to be sensitive to the roughness of the heated surface; this study uses a correlation that does not explicitly consider surface roughness. Nucleate pool boiling heat transfer coefficient (h_{PB}) data for water were correlated with heat flux (q_{PB}), critical pressure (P_c) and reduced pressure (P_R) by *Mostinski* [1963]:

$$h_{PB} = 0.106 P_c^{0.69} \left(1.8 P_R^{0.17} + 4 P_R^{1.2} + 10 P_R^{10}\right) q_{PB}^{2/3} \tag{B1}$$

where P_R = system pressure/critical pressure and the units used are W m^{-2} K^{-1} for h_{PB}, W m^{-2} for q_{PB} and bar (1 bar = 0.1 MPa) for P_c. The heat flux versus ΔT correlation can be developed by recalling that

$$q_{PB} = h_{PB} \Delta T \tag{B2}$$

$$\text{whence } q_{PB} = B \Delta T^3 \tag{B3}$$

where B is a constant for nucleate pool boiling at a fixed pressure.

[77] *Whalley* [1987, p. 134] discussed the effect of liquid velocity on nucleate boiling. Forced convection heat transfer for single phase flow over spheres can be described by Whitaker's equation [*Whitaker*, 1972; *Incropera and DeWitt*, 1996, p. 349]:

$$Nu = 2 + \left(0.4 Re^{1/2} + 0.06 Re^{2/3}\right) Pr^{0.4} \tag{B4}$$

where the Nusselt number Nu is defined as $h_{FC}\ d/k_f$, the Reynolds number Re as $V\ \rho\ d/\mu$ and the Prandtl number Pr as $\mu\ C_p/k_f$, with forced convection heat transfer coefficient h_{FC}, sphere diameter d, fluid velocity (relative to particle surface) V and with k_f, ρ, μ and C_p being the fluid thermal conductivity, density, viscosity and specific heat capacity respectively. The forced convection heat flux is then:

$$q_{FC} = h_{FC} \Delta T \tag{B5}$$

The nucleate pool boiling heat flux and the forced convective heat flux may be combined to give an expression for the total nucleate boiling heat flux q_{NB}:

$$q_{NB} = \left(q_{PB}^2 + q_{FC}^2\right)^{1/2} \quad \text{(B6)}$$

B2. Critical Heat Flux

[78] The critical heat flux $q_{\max}$ for cylinders of radius R can be estimated from equation (B7) [*Sun and Lienhard*, 1970; *Whalley*, 1987, p 141]:

$$q_{\max} = \alpha\lambda\rho_g^{1/2}\left[g\sigma_f\left(\rho_l - \rho_g\right)\right]^{1/4} \quad \text{(B7)}$$

$$\text{where } \alpha = 0.116 + 0.3\exp\left\{-3.44R^{1/2}\left[\frac{g\left(\rho_l - \rho_g\right)}{\sigma_f}\right]^{1/4}\right\} \quad \text{(B8)}$$

and λ, ρ_g, ρ_l and σ_f are the fluid latent heat of vaporization, vapor density, liquid density and surface tension respectively and g is the acceleration due to gravity.

[79] *Lienhard and Lienhard* [2008, p. 484] compared data for cylinders and spheres. Based on this comparison, equation (B7) is accurate for large ($R > 5$ mm) spheres but increasingly tends to underestimate $q_{\max}$ as radius decreases.

B3. Film Boiling Regime

[80] In this regime, heat transfer is by radiation and convection [*Bromley*, 1950; *Whalley*, 1987, p. 192]. The radiation heat transfer coefficient is determined by:

$$h_R = \varepsilon\sigma\left(\frac{T_S^4 - T_b^4}{T_S - T_b}\right) \quad \text{(B9)}$$

where ε is the particle surface emissivity, σ is the Stefan-Boltzmann constant, T_S is the particle surface temperature and T_b is the boiling liquid bulk temperature.

[81] To model the convective heat transfer, *Bromley et al.* [1953] defined a modified Froude number:

$$Fr = \frac{V^2}{gd} \quad \text{(B10)}$$

where V is the fluid velocity relative to the particle, d the particle diameter and g the acceleration due to gravity, and they use this to distinguish the cases of (1) pool film boiling and (2) flow film boiling. For pool film boiling ($Fr < 1$), the convection heat transfer coefficient is given by:

$$h_{FB} = 0.62\left[\frac{g\lambda k_g^3\rho_g\left(\rho_l - \rho_g\right)}{d\Delta T\mu_g}\right]^{1/4} \quad \text{(B11)}$$

where ρ_l is the liquid density, ρ_g is the vapor density, k_g is the vapor thermal conductivity, μ_g is the vapor viscosity, λ is the latent heat of vaporization and ΔT is the temperature difference between the particle surface and the bulk fluid. The combined radiative and convective film boiling heat transfer coefficient is given by:

$$h_{TOT} = h_{FB} + 0.75h_R \quad \text{(B12)}$$

For flow film boiling ($Fr > 4$), the convection heat transfer coefficient is given by:

$$h_{FB} = 2.7\left(\frac{\rho_g V\lambda k_g}{d\Delta T}\right)^{1/2} \quad \text{(B13)}$$

The combined radiative and convective film boiling heat transfer coefficient is given by:

$$h_{TOT} = h_{FB} + 0.875h_R \quad \text{(B14)}$$

Although equations (B10)–(B14) were developed for cylinders, they can be applied to spheres without significant loss of accuracy [*Lienhard and Lienhard*, 2008, p. 486].

[82] In both cases, the film boiling heat flux is given by:

$$q_{FB} = h_{TOT}\Delta T \quad \text{(B15)}$$

We note that the boiling heat transfer equations were developed from experiments carried out under steady conditions. Steady film boiling is characterized by a stable vapor film that separates the hot surface from the bulk liquid. During explosive volcanic eruptions the collapse of the stable film could be triggered by external shock waves from magmatic and phreatomagmatic explosions [*Zimanowski and Büttner*, 2003].

B4. Minimum Film Boiling Temperature

[83] For water, minimum film boiling temperature $T_{\min}$ (in °C) can be correlated with saturation pressure P (in bars) [*Groeneveld and Stewart*, 1982]:

$$T_{\min} = 285 + 4.41P - 0.0372P^2 \text{ for } P < 90 \text{ bar (9 MPa)} \quad \text{(B16)}$$

$\Delta T_{\min}$ is then evaluated from:

$$\Delta T_{\min} = T_{\min} - T_b \quad \text{(B17)}$$

where T_b is the boiling liquid bulk temperature.

B5. Transition Boiling Regime

[84] *Whalley* [1987, p. 256] suggested a straight line interpolation between the critical heat flux condition and the onset of film boiling on a log-log plot of heat flux q and ΔT:

$$q' = q'_{\max} - \left(\frac{q'_{\max} - q'_{\min}}{\Delta T'_{\min} - \Delta T'_{CHF}}\right)\left(\Delta T' - \Delta T'_{CHF}\right) \quad \text{(B18)}$$

where the primed symbol (′) indicates the log of a variable (e.g., $q' = \log q$), $q_{\max}$ and ΔT_{CHF} are the heat flux and surface temperature difference at critical heat flux conditions, $\Delta T_{\min}$ is defined in equation (B17) and $q_{\min}$ is the heat flux at $\Delta T_{\min}$.

B6. Summary

[85] The heat flux versus ΔT equations for the nucleate, transition and film boiling regimes, together with the values for critical heat flux and $\Delta T_{\min}$, fully define the heat flux

versus ΔT equations used within the numerical model developed in Section 2 of the paper.

Notation

B constant in nucleate pool boiling equation, W m^{-2} K^{-3}
Bi Biot number (defined as $U\,d\,/2\,k$ or $U\,r_o\,/k$), dimensionless
C_p fluid specific heat capacity, J kg^{-1} K^{-1}
D particle fragmentation exponent, dimensionless
d particle diameter, m
Fo Fourier number (defined as $K\,t/r_o^2$), dimensionless
Fr Froude number (defined as $V^2/g\,d$), dimensionless
g acceleration due to gravity, m s^{-2}
h_{FB} film boiling convection heat transfer coefficient, W m^{-2} K^{-1}
h_{FC} forced convection heat transfer coefficient, W m^{-2} K^{-1}
h_{PB} nucleate pool boiling heat transfer coefficient, W m^{-2} K^{-1}
h_R radiation heat transfer coefficient, W m^{-2} K^{-1}
h_{TOT} combined film boiling heat transfer coefficient, W m^{-2} K^{-1}
K particle thermal diffusivity, m^2 s^{-1}
k particle thermal conductivity, W m^{-1} K^{-1}
k_f thermal conductivity of the fluid phase surrounding the particle, W m^{-1} K^{-1}
k_g vapor thermal conductivity, W m^{-1} K^{-1}
N number of fragments with radii greater than r, dimensionless
Nu Nusselt number (defined as $U\,d/k_f$), dimensionless
P saturation pressure, Pa
P_c critical pressure, Pa
P_R reduced pressure (=system pressure/critical pressure), dimensionless
Pr Prandtl number (defined as $\mu\,C_p/k_f$), dimensionless
Q/Q_i fractional heat loss from particle, dimensionless
q boiling heat flux at particle surface, W m^{-2}
q_{FB} film boiling heat flux, W m^{-2}
q_{FC} forced convection heat flux, W m^{-2}
$q_{\max}$ critical heat flux, W m^{-2}
$q_{\min}$ heat flux at $\Delta T_{\min}$, W m^{-2}
q_{NB} total nucleate boiling heat flux, W m^{-2}
q_{PB} nucleate pool boiling heat flux, W m^{-2}
R cylinder radius, m
Re Reynolds number (defined as $V\,\rho\,d/\mu$), dimensionless
r particle radial coordinate, m
r_o particle radius, m
T internal temperature of particle, K
T_b boiling liquid bulk temperature, K
T_e mean temperature of sample before burial, K
$T_{\min}$ minimum film boiling temperature, K
T_S particle surface temperature, K
t particle cooling time or thermal "diffusion time," s
U particle surface heat transfer coefficient, W m^{-2} K^{-1}
V fluid velocity (relative to particle surface), m s^{-1}
V_t total volume of ice melted, km^3
ΔT temperature difference between the surface and the boiling liquid, K
ΔT_{CHF} temperature difference at critical heat flux, K
$\Delta T_{\min}$ minimum film boiling temperature difference, K
α constant in critical heat flux equation, dimensionless
β constant in particle fragmentation equation, m^D
ε particle surface emissivity, dimensionless
λ fluid latent heat of vaporization, J kg^{-1}
μ fluid viscosity, Pa s
μ_g vapor viscosity, Pa s
ρ fluid density, kg m^{-3}
ρ_g vapor density, kg m^{-3}
ρ_l liquid density, kg m^{-3}
σ Stefan-Boltzmann constant, W m^{-2} K^{-4}
σ_f surface tension, N m^{-1}

[86] **Acknowledgments.** We sincerely thank Magnus Tumi Gudmundsson for his detailed comments which have greatly improved the paper. We also thank an anonymous reviewer, the Editor André Revil and the Associate Editor for their help. We are grateful to Lionel Wilson for comments on an early version of this paper.

References

Allen, S. R., and J. McPhie (2009), Products of Neptunian eruptions, *Geology*, *37*, 639–642, doi:10.1130/G30007A.1.

Anderson, J. D. (1995), *Computational Fluid Dynamics*, McGraw Hill, New York.

Bagdassarov, N., and D. Dingwell (1994), Thermal properties of vesicular rhyolite, *J. Volcanol. Geotherm. Res.*, *60*, 179–191, doi:10.1016/0377-0273(94)90067-1.

Ball, M., and H. Pinkerton (2006), Factors affecting the accuracy of thermal imaging cameras in volcanology, *J. Geophys. Res.*, *111*, B11203, doi:10.1029/2005JB003829.

Birnie, D. P., and M. D. Dyar (1986), Cooling rate calculations for silicate glasses, *J. Geophys. Res.*, *91*, D509–D513, doi:10.1029/JB091iB04p0D509.

Bromley, L. A. (1950), Heat transfer in stable film boiling, *Chem. Eng. Prog.*, *46*, 221–227.

Bromley, L. A., N. R. LeRoy, and J. A. Robbers (1953), Heat transfer in forced convection film boiling, *Ind. Eng. Chem.*, *49*, 1921–1928.

Capaccioni, B., and F. Cuccoli (2005), Spatter and welded air fall deposits generated by fire-fountaining eruptions: Cooling of pyroclasts during transport and deposition, *J. Volcanol. Geotherm. Res.*, *145*, 263–280, doi:10.1016/j.jvolgeores.2005.02.001.

Carslaw, H. S., and J. C. Jaeger (1959), *Conduction of Heat in Solids*, Clarendon, Oxford.

Cas, R. A. F., and J. V. Wright (1991), Subaqueous pyroclastic flows and ignimbrites: An assessment, *Bull. Volcanol.*, *53*, 357–380, doi:10.1007/BF00280227.

Cioni, R., A. Sbrana, and R. Vecci (1992), Morphologic features of juvenile pyroclasts from magmatic and phreatomagmatic deposits of Vesuvius, *J. Volcanol. Geotherm. Res.*, *51*, 61–78, doi:10.1016/0377-0273(92)90060-Q.

Grober, H., S. Erk, and U. Grigull (1961), *Fundamentals of Heat Transfer*, McGraw Hill, New York.

Groeneveld, D. C., and J. C. Stewart (1982), The minimum film boiling temperature for water during film boiling collapse, in *Heat Transfer 1982: Proceedings of the 7th International Heat Transfer Conference*, vol. 4, pp. 393–398, Hemisphere Publ., Washington, D. C.

Gudmundsson, M. T. (2003), Melting of ice by magma-ice-water interactions during subglacial eruptions as an indicator of heat transfer in subaqueous eruptions, in *Explosive Subaqueous Volcanism*, *Geophys. Monogr. Ser*, vol. 140, edited by J. D. L. White, J. L. Smellie, and D. A. Clague, pp. 61–72, AGU, Washington, D.C., doi:10.1029/140GM04

Gudmundsson, M. T., F. Sigmundsson, and H. Bjornsson (1997), Ice–volcano interaction of the 1996 Gjálp subglacial eruption, Vatnajökull, Iceland, *Nature*, *389*, 954–957, doi:10.1038/40122.

Gudmundsson, M. T., F. Palsson, H. Bjornsson, and T. Hognadottir (2002), The hyaloclastite ridge formed in the subglacial 1996 eruption in Gjálp, Vatnajökull, Iceland: Present day shape and future preservation, *Geol. Soc. Spec. Publ.*, *202*, 319–335.

Gudmundsson, M. T., F. Sigmundsson, H. Bjornsson, and T. Hognadottir (2004), The 1996 eruption at Gjálp, Vatnajökull ice cap, Iceland:

Efficiency of heat transfer, ice deformation and subglacial water pressure, *Bull. Volcanol.*, *66*, 46–65, doi:10.1007/s00445-003-0295-9.
Head, J. W., and L. Wilson (2003), Deep submarine pyroclastic eruptions: Theory and predicted landforms and deposits, *J. Volcanol. Geotherm. Res.*, *121*, 155–193, doi:10.1016/S0377-0273(02)00425-0.
Heisler, M. P. (1947), Temperature charts for induction and constant temperature heating, *Trans. Am. Soc. Mech. Eng.*, *69*, 227–236.
Höskuldsson, A., and R. S. J. Sparks (1997), Thermodynamics and fluid dynamics of effusive subglacial eruptions, *Bull. Volcanol.*, *59*, 219–230, doi:10.1007/s004450050187.
Incropera, F. P., and D. P. DeWitt (1996), *Introduction to Heat Transfer*, John Wiley, New York.
Jakobsson, S. P., and M. T. Gudmundsson (2008), Subglacial and intraglacial volcanic formations in Iceland, *Jökull*, *58*, 179–196.
Jarosch, A., M. T. Gudmundsson, T. Hognadottir, and G. Axelsson (2008), Progressive cooling of the hyaloclastite ridge at Gjálp, Iceland, 1996–2005, *J. Volcanol. Geotherm. Res.*, *170*, 218–229, doi:10.1016/j.jvolgeores.2007.10.012.
Kaminski, E., and C. Jaupart (1998), The size distribution of pyroclasts and the fragmentation sequence in explosive volcanic eruptions, *J. Geophys. Res.*, *103*, 29,759–29,779, doi:10.1029/98JB02795.
Keszthelyi, L., and R. Denlinger (1996), The initial cooling of pahoehoe flow lobes, *Bull. Volcanol.*, *58*, 5–18, doi:10.1007/s004450050121.
Kokelaar, B. P., and G. P. Durant (1983), The submarine eruption and erosion of Surtla (Surtsey), Iceland, *J. Volcanol. Geotherm. Res.*, *19*, 239–246, doi:10.1016/0377-0273(83)90112-9.
Kreith, F., and M. S. Bohn (1993), *Principles of Heat Transfer*, West Publ., St Paul, Minn.
Lienhard, J. H., and J. H. Lienhard (2008), *A Heat Transfer Textbook*, Phlogiston, Cambridge, U. K.
Mastin, L. (2007), Generation of fine hydromagmatic ash by growth and disintegration of glassy rinds, *J. Geophys. Res.*, *112*, B02203, doi:10.1029/2005JB003883.
Mostinski, I. L. (1963), Calculation of heat transfer and critical heat flux in boiling liquids based on the law of corresponding states, *Teploenergetika*, *10*, 66–71.
Murase, T., and A. R. McBirney (1973), Properties of some common igneous rocks and their melts at high temperatures, *Geol. Soc. Am. Bull.*, *84*, 3563–3592, doi:10.1130/0016-7606(1973)84<3563:POSCIR>2.0.CO;2.
Pierson, T. C., R. J. Janda, J.-C. Thouret, and C. A. Borrero (1990), Perturbation and melting of snow and ice by the 13 November 1985 eruption of Nevado del Ruiz, Colombia, and consequent mobilization, flow and deposition of lahars, *J. Volcanol. Geotherm. Res.*, *41*, 17–66, doi:10.1016/0377-0273(90)90082-Q.
Rogers, G. F. C., and Y. R. Mayhew (1980), *Thermodynamic and Transport Properties of Fluids (SI Units)*, Blackwell, Oxford, U. K.
Skilling, I. P., J. D. L. White, and J. McPhie (2002), Peperite: A review of magma-sediment mingling, *J. Volcanol. Geotherm. Res.*, *114*, 1–17, doi:10.1016/S0377-0273(01)00278-5.
Sparks, R. S. J., M. I. Bursik, S. N. Carey, J. S. Gilbert, L. S. Glaze, H. Sigurdsson, and A. W. Woods (1997), *Volcanic Plumes*, Wiley, Chichester, U. K.
Spera, F. J. (2000), Physical properties of magmas, in *Encyclopaedia of Volcanoes*, edited by H. Sigurdsson, pp. 171–190, Academic, San Diego, Calif.
Steinthorsson, S., B. S. Hardarson, R. M. Ellam, and G. Larsen (2000), Petrochemistry of the Gjálp 1996 subglacial eruption, Vatnajökull, SE Iceland, *J. Volcanol. Geotherm. Res.*, *98*, 79–90, doi:10.1016/S0377-0273(99)00186-9.
Stevenson, J. A., J. S. Gilbert, D. W. McGarvie, and J. L. Smellie (2011), Explosive rhyolite tuya formation: Classic examples from Kerlingarfjöll, Iceland, *Quat. Sci. Rev.*, *30*, 192–209, doi:10.1016/j.quascirev.2010.10.011.
Sun, K. H., and J. H. Lienhard (1970), The peak pool boiling heat flux on horizontal cylinders, *Int. J. Heat Mass Transfer*, *13*, 1425–1439, doi:10.1016/0017-9310(70)90178-X.
Thomas, R. M. E., and R. S. J. Sparks (1992), Cooling of tephra during fallout from eruption columns, *Bull. Volcanol.*, *54*, 542–553, doi:10.1007/BF00569939.
Tweed, F., M. J. Roberts, and A. J. Russell (2005), Hydrologic monitoring of supercooled meltwater from Icelandic glaciers, *Quat. Sci. Rev.*, *24*, 2308–2318, doi:10.1016/j.quascirev.2004.11.020.
Whalley, P. B. (1987), *Boiling, Condensation, and Gas-Liquid Flow*, Clarendon, Oxford, U. K.
Whitaker, S. (1972), Forced convection heat transfer correlations for flow in pipes, past flat plates, single cylinders, single spheres, and for flow in packed beds and tube bundles, *AIChE. J.*, *18*, 361–371, doi:10.1002/aic.690180219.
Zimanowski, B., and R. Büttner (2003), Phreatomagmatic explosions in subaqueous volcanism, in *Explosive Subaqueous Volcanism*, *Geophys. Monogr. Ser*, vol. 140, edited by J. D. L. White, J. L. Smellie, and D. A. Clague, pp. 51–60, AGU, Washington, D.C., doi:10.1029/140GM03.